Robotica (1989) volume 7, pp 143–149

Statically balanced direct drive manipulator

H. Kazerooni

Mechanical Engineering Department, University of Minnesota, 111 Church Street S.E. Minneapolis, MN 55455 (USA)

(Received in Final Form: July 29, 1988)

SUMMARY

A practical architecture, using a four-bar-linkage, is considered for the University of Minnesota direct drive rotot[1]. This statically-balanced direct drive robot has been constructed for stability analysis of the robot in constrained maneuvers.[2–6] As a result of the elimination of the gravity forces (without any counter weights), smaller actuators and consequently smaller amplifiers were chosen. The motors yield acceleration of 5 g at the robot end point without overheating. High torque, low speed, brush-less AC synchronous motors are used to power the robot. Graphite-epoxy composite material is used for the construction of the robot links. A 4-node parallel processor has been used to control the robot. The dynamic tracking accuracy-with the feedforward torque method as a control law- has been derived experimentally.

KEYWORDS: Direct drive; Robot; Statically balanced; Tracking accuracy; Linkage.

INTRODUCTION

The work presented here is on the design and control of the Minnesota direct drive robot. This robot is statically balanced and uses a four bar link mechanism to compensate for some of the drawbacks of serial type[7] and parallelogram type[8] direct drive robots. Before describing the properties of this arm, some disadvantages and advantages of direct drive arms are discussed here as follows:

1. *Speed.* The maneuvering speed of the direct drive arms is not necessarily greater than the non-direct drive robot arms. The maximum achievable speed for a given architecture depends on the transmission ratio. The optimum transmission ratio is a function of the inertia of the links. A simple example in apprndix A shows that for a given architecture, a non-direct drive arm can be faster than a direct drive arm.
2. *Static Payload.* It is obvious that for a given set of motors, direct drive arms will have a lower static payload than non-direct drive arms. This is because of the inherent evident property of reducer transmission systems.
3. *Overheating.* Elimination of the transmission system causes the inertial force and the gravitational force of the links affect the motors directly. In other words, the motors "feel" the inertial and the gravitational forces without any reduction in size. The direct effect of the forces cause the motors to overheat in the direct drive arms. This overheating exists even in the static case when the arm is only under its static load.
4. *Structural Stiffness.* The structural stiffness of the direct drive arms is greater than the non-direct drive systems. About 80% of the total mechanical compliance in most non-direct drive industrial robots is caused by transmission systems[9,10]. The high structural stiffness allows for wide bandwidth control. The low structural stiffness of non-direct drive arms, due to the existence of many mechanical elements in the transmission system, is a limiting factor on achievement of a relatively wide bandwidth control system.
5. *Backlash and Friction.* The direct drive arms are free from mechanical backlash and friction due to elimination of transmission systems. A small mechanical backlash in the transmission system would cause the gear teeth to wear faster. The high rate of wear in the gear would develop an even larger backlash. About 25% of the torque in non direct drive arms is used to overcome the friction.[11]
6. *Performance and Control.* Because of elimination of the transmission systems, and consequently backlash, the control and performance analysis of direct drive arms is more straightforward than the non-direct drive arms (not necessarily "easier").
7. *Accuracy.* The accuracy of direct drive arms is questionable. The lack of the transmission system eliminates cogging, backlash, and its corresponding limit cycle in the control system. On the other hand, the motor vibrations in the direct drive systems are directly transferred to the robot end point.

Several attempts have been made to improve the manipulator dynamic behavior. Asada and Kanade[7] designed a serial type direct drive arm in which the actuators were directly coupled to links without any transmission mechanism. The elimination of the transmission mechanism improved the robot performance, however large motors were needed to drive the robot. Asada and Youcef-Toumi[8] studied a direct drive arm with a parallelogram mechanism to eliminate the problems associated with serial type robots. A direct drive arm with a counterweight was designed by Takase et al.[12] in order to eliminate the gravity effect at three major joints. Another direct drive arm, designed by Kuwahara et al.[13] to reduce the effect of gravity using a four bar link for the forearm, and a special spring for the upper arm. The counterweight provides the system balance for all possible positions, however, it increases the total inertia of the robot arm. The spring balancing will not perfectly balance the system either[14].

University of Minnesota direct drive robot arm.

In this research, a statically balanced direct drive arm is designed to achieve improved dynamic behavior (Figures 1 and 2). As a result of the elimination of the gravity forces (without any counter weights), smaller actuators and consequently smaller amplifiers were chosen. The motors yield acceleration of 5 g at the end point without overheating.

ARCHITECTURE

The architecture of this arm is such that the gravity term is completely eliminated from the dynamic equations. This balanced mechanism is designed without adding any extra counterbalance weights. The new features of this new design are as follows:

1. Since the motors are never affected by gravity, the static load will be zero. Hence no overheating results in the system in the static case.
2. The elimination of gravity terms calls for smaller motors with less stall torque (and consequently smaller amplifiers) which have been chosen for a desired acceleration.

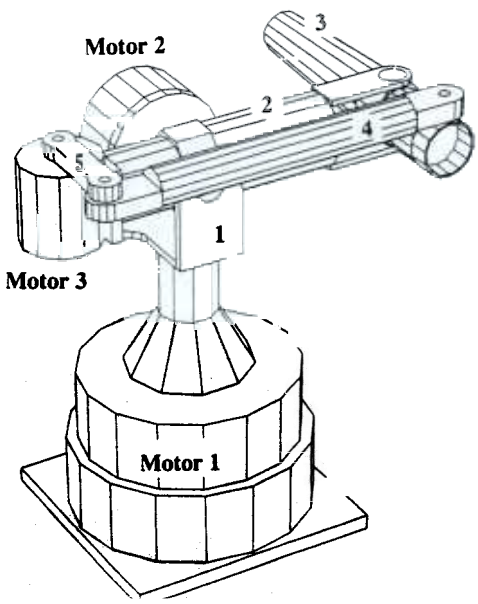

University of Minnesota Direct Drive Robot

Schematic of university of Minnesota arm

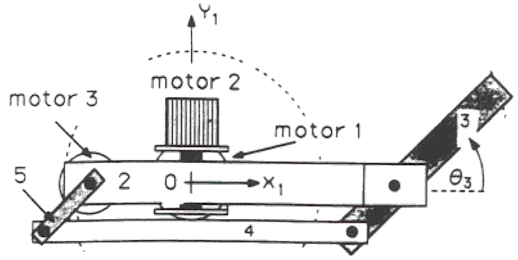

Top View

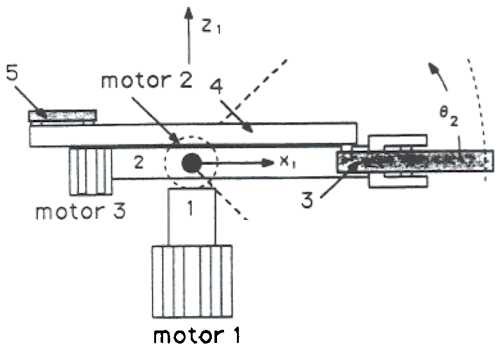

Side View

Fig. 3. The side view and top view of the robot.

3. With the lack of gravity terms, higher accuracy can be achieved. This is true because the links have steady deflection due to constant gravity effect. This gives better accuracy and repeatability for fine manipulation tasks.
4. As depicted in Figure 3, the architecture of this robot allows for a "large" workspace. The horizontal workspace (radius = 80 cm) of this robot is quite attractive from the stand point of manufacturing tasks such as assembly and deburring.
5. Graphite-epoxy composite material is used for the construction of the robot links. This robot is light (60 kg) and can be mounted on an autonomous vehicle. The pay load without losing precision is 2 kg.

Figure 2 shows the schematic diagram of the University of Minnesota direct drive arm. The arm has three degrees of freedom, all of which are articulated drive joints. Motor 1 powers the system about a vertical axis. Motor 2 pitches the entire four-bar-linkage while motor 3 is used to power the four-bar-linkage. Link 2 is directly connected to the shaft of motor 2. Figure 3 shows the top view and side view of the robot. The

coordinate frame $X_iY_iZ_i$ has been assigned to link i of the robot for $i = 1, 2, \ldots, 5$. The center of coordinate frame $X_1Y_1Z_1$ corresponding to link 1 is located at point O as shown in figure 3. The center of the inertial global coordinate frame $X_0Y_0Z_0$ is also located at point O (The global coordinate frame is not shown in the figures). The joint angles are represented by θ_1, θ_2, and θ_3. θ_1 represents the rotation of link 1; coordinate frame $X_1Y_1Z_1$ coincides on global coordinate frame $X_0Y_0Z_0$ when $\theta_1 = 0$. θ_2 represents the pitch angle of the four-bar-linkage as shown in Figure 3. θ_3 represents the angle between link 2 and link 3. Shown are the conditions under which the gravity terms are eliminated from the dynamic equations.

Figure 4 shows the four-bar-linkage with assigned coordinate frames. By inspection the conditions under which the vector of gravity passes through origin, O, for all possible values of θ_1 and θ_3 are given by equations (1) and (2).

$$(m_3\bar{x}_3 - m_4L_5 - m_5\bar{x}_5)\sin\theta_3 = 0 \quad (1)$$

$$g(mt_3 + m_5) - m_2\bar{x}_2 - m_3(L_2 - g) - m_4(\bar{x}_4 - g) - (m_3\bar{x}_3 - m_4L_5 - m_5\bar{x}_5)\cos\theta_3 = 0 \quad (2)$$

where

m_i, L_i = mass and length of each link,
$\bar{x}_i$ = the distance of center of mass from the origin of each coordinate frame,
mt_3 = mass of motor 3.

Conditions (1) and (2) result in:

$$m_3\bar{x}_3 - m_4L_5 - m_5\bar{x}_5 = 0 \quad (3)$$

$$g(mt_3 + m_5) - m_2\bar{x}_2 - m_3(L_2 - g) - M_4(\bar{x}_4 - g) = 0 \quad (4)$$

If equations (3) and (4) are satisfied, then the center of gravity of the four-bar-linkage passes through point O for all the possible configurations of the arm. Note that the gravity force still passes through O even if the plane of the four-bar-linkage is tilted by motor 2 for all values of θ_2. The values for various parameters are given in Appendix B.

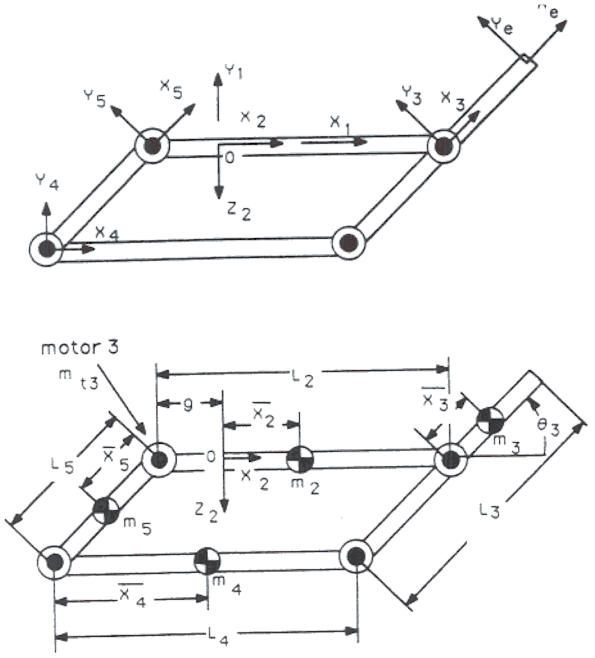

Fig. 4. Four bar link mechanism.

Since at low speeds, AC torque motors do not tend to cog, low speed, high torque, and brush-less AC synchronous motors have been chosen to power the robot. Each motor consists of a ring shaped stator and a ring shaped permanent magnet rotor with a large number of poles. The rotor is made of rare earth magnetic material (Neodymium) bonded to a low carbon steel yoke with structural adhesive. The stator of the motor (with winding) is fixed to the housing for heat dissipation. To develop wide bandwidth (high speed) closed loop control for the robot, Graphite-expoxy composite and AA7075T6 Materials were used to construct the links. The high structural stiffness and low density of the Graphite-expoxy composite result in high natural frequencies in the robot dynamics. The higher the natural frequencies are, the wider the bandwidth and consequently faster the closed loop system will be[15]. A strong bond between the composite parts and the aluminum parts was achieved using an epoxy adhesive (3M Epoxy Adhesive EC-3569 B/A). To minimize joint clearance and reduce bearing mass, Super Precision angular contact bearings (ABEC-7, extremely light series 1900) were used.

FORWARD KINEMATICS

The forward kinematic problem is to compute the position of the end point in the global coordinate frame $X_0Y_0Z_0$, given the joint angles, θ_1, θ_2, and θ_3. The end point position of the robot relative to the global coordinate frame is characterized by P_x, P_y, and P_z in the global coordinate frame $X_0Y_0Z_0$:

$$P_x = (C_1C_2C_3 - S_1S_3)(L_3 - L_5) + C_1C_2(L_2 - g) \quad (5)$$

$$P_y = (S_1C_2C_3 + C_1S_3)(L_3 - L_5) + S_1C_2(L_2 - g) \quad (6)$$

$$P_z = S_2(L_2 - g) + S_2C_3(L_3 - L_5) \quad (7)$$

where $S_i = \mathrm{Sin}(\theta_i)$, and $C_i = \mathrm{Cos}(\theta_i)$.

INVERSE KINEMATICS

The inverse kinematic problem is to calculate the joint angles for a given end point position with respect to the global coordinate frame. The closed-form of inverse kinematics of the proposed arm derived using the standard method[11,16]. The joint angles for the given end point position can be determined using the following equations:

$$\theta_1 = \mathrm{atan}\,2(P_y, P_x) - \mathrm{atan}\,2((L_3 - L_5)\sin\theta_3 \pm \sqrt{P_x^2 + P_y^2 - (L_3 - L_5)^2\sin^2\theta_3}) \quad (8)$$

$$\theta_2 = \sin^{-1}\left(\frac{P_z}{(L_2 - g) + (L_3 - L_5)\cos\theta_3}\right) \quad (9)$$

$$\theta_3 = \cos^{-1}\left(\frac{P_x^2 + P_y^2 + P_z^2 - (L_2 - g)^2 - (L_3 - L_5)^2}{2(L_2 - g)(L_3 - L_5)}\right) \quad (10)$$

DYNAMICS

The closed-form dynamic equations have been derived for the purpose of controller design. The dynamic behavior of the arm can be presented by the following equation[17,18]

$$M(\theta)\ddot{\theta} + CE(\theta)(\dot{\theta}^2) + CO(\theta)(\dot{\theta}\dot{\theta}) + G(\theta) = \tau \quad (11)$$

where:

$\tau = (\tau_1 \tau_2 \tau_3)^T$ 3×1 vector of the motor torques,
$M(\theta)$ 3×3 definite inertia matrix,
$CE(\theta)$ 3×3 centrifugal coefficients matrix,
$CO(\theta)$ 3×3 Coriolis coefficients matrix,
$G(\theta)$ 3×1 vector of gravity force,
$\ddot{\theta}$ $(\ddot{\theta}_1 \quad \ddot{\theta}_2 \quad \ddot{\theta}_3)^T$
$(\dot{\theta}\dot{\theta})$ $(\dot{\theta}_1\dot{\theta}_2 \quad \dot{\theta}_1\dot{\theta}_3 \quad \dot{\theta}_2\dot{\theta}_3)^T$
$(\dot{\theta}^2)$ $(\dot{\theta}_1^2 \quad \dot{\theta}_2^2 \quad \dot{\theta}_3^2)^T$

$$M(\theta) = \begin{pmatrix} & & \\ & & \\ & & \end{pmatrix}, \qquad \begin{pmatrix} 0 & CE_{12} & CE_{13} \\ CE_{21} & 0 & 0 \\ CE_{31} & CE_{32} & 0 \end{pmatrix}$$

$$CO(\theta) = \begin{pmatrix} CO_{11} & CO_{12} & CO_{13} \\ 0 & CO_{22} & CO_{23} \\ CO_{31} & 0 & 0 \end{pmatrix}, \qquad G(\theta) = \begin{pmatrix} 0 \\ 0 \\ 0 \end{pmatrix}$$

$$M_{11} = I_{z1} + C_2^2(I_{e1} + I_{e6} + I_{e2} + 2C_3 I_{e3} + I_{y2} + m_2\bar{x}_2^2) + S_2^2(S_3^2(I_{e1} + I_{e5}) + C_3^2 I_{e4} + I_{x2})$$

$$M_{12} = S_2 S_3(I_{e3} + C_3(I_{e1} + I_{e5} - I_{e4}))$$

$$M_{13} = C_2(I_{e1} + I_{e6} + C_3 I_{e3})$$

$$M_{22} = I_{z2} + m_2\bar{x}_2^2 + C_3^2(I_{e1} + I_{e5}) + S_3^2 I_{e4} + I_{e2} + 2C_3 I_{e3}$$

$$M_{33} = I_{e1} + I_{e6}$$

$$CE_{12} = C_2 S_3(I_{e3} + C_3(I_{e1} + I_{e5} - I_{e4}))$$

$$CE_{13} = -C_2 S_3 I_{e3}$$

$$CE_{21} = S_2 C_2(I_{y2} - I_{x2} + m_2\bar{x}_2^2 - S_3^2 I_{e5} + C_3^2(I_{e1} - I_{e4}) + I_{e2} + I_{e6} + 2C_3 I_{e3})$$

$$CE_{31} = S_3(C_2^2 I_{e3} - S_2^2 C_3(I_{e1} + I_{e5} - I_{e4}))$$

$$CE_{32} = S_3(I_{e3} + C_3(I_{e1} + I_{e5} - I_{e4}))$$

$$CO_{11} = -2CE_{21}$$

$$CO_{12} = -2CE_{31}$$

$$CO_{13} = -S_2(2S_3^2 I_{e1} + I_{e6} + \cos 2\theta_3(I_{e4} - I_{e5}))$$

$$CO_{22} = S_2(2C_3^2 I_{e1} + I_{e6} + 2C_3 I_{e3} - \cos 2\theta_3(I_{e4} - I_{e5}))$$

$$CO_{23} = -2CE_{32}$$

$$CO_{31} = -S_2(I_{e1} + \cos 2\theta_3[I_{e1} + I_{e5} - I_{e4}) + I_{e6} + 2C_3 I_{e3})$$

where:

$$I_{e1} = m_3\bar{x}_3^2 + m_4 L_5^2 + m_5\bar{x}_5^2$$

$$I_{e2} = m_3(L_2 - g)^2 + m_4(\bar{x}_4 - g)^2 + m_5 g^2$$

$$I_{e3} = m_3\bar{x}_3(L_2 - g) - m_4(\bar{x}_4 - g)L_5 + m_5\bar{x}_5 g$$

$$I_{e4} = I_{x3} + I_{x4} + I_{x5}$$

$$I_{e5} = I_{y3} + I_{y4} + I_{y5}$$

$$I_{e6} = I_{z3} + I_{z4} + I_{z5}$$

I_{xi}, I_{yi}, and I_{zi} are the mass moments of inertia relative to x, y, z axis at the center of mass of a link i. (motor 3 is a part of link 2). The gravity term, $G(\theta)$ becomes zero when equations (3) and (4) are satisfied in the arm. This condition holds for all possible configurations.

HARDWARE

A schematic of the system hardware is shown in Figure 5. An IBM AT microcomputer which is hosting a 4-node NCUBE parallel processor is used as the main controller of this robot. The parallel processor has four nodes and a PC/AT bus interface. Each node is an independent 32-bit processor with local memory and communication links to the other nodes in the system. A high speed AD/DA converter has been used for reading the velocity signals and sending analog command signals to the servo controller unit. A parallel IO board (D/D converter) between the servo controller unit and the computer allows for reading the R/D (Resolver to Digital) converter.

The servo controller unit produces three phase, Pulse Width Modulated (PWM), sinusoidal currents for the power amplifier. The servo controller unit contains an interpolator, R/D converter and a communication interface for the computer. The servo controller unit can be operated in either a closed loop velocity or current (torque) control mode (the current control is used). A PWM power amplifier, which provides up to 47 Amperes of drive current from a 325 volt power supply, is used to power the motors. The main DC bus power is derived by full-wave rectifying the three phase 230 VAC incoming power. This yields a DC bus voltage of 325 VDC.

The actuators used in this robot are neodymium (NdFeB) magnet AC brushless synchronous motors. Due to the high magnetic field strength (maximum energy products: 35 MGOe) of the rare earth NdFeB magnets, the motors have high torque to weight ratio. Pancake type resolvers are used as position and velocity sensors. The peak torque of motor 1 is 118 Nm, while the peak torques of motors 2 and 3 are 78 and 58 Nm, respectively.

IDENTIFICATION OF DYNAMIC PARAMETERS

The dynamic parameters used in control were experimentally identified by a dynamic parameter identification method developed in ref. 19. The identification

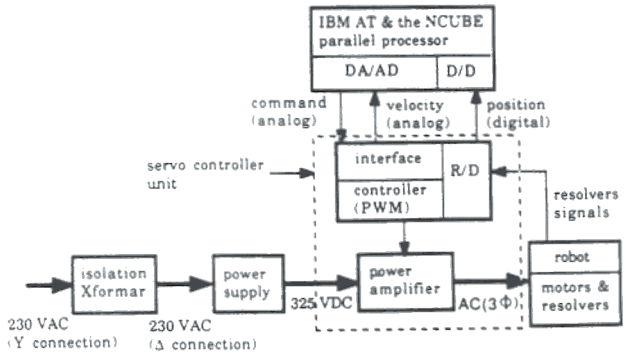

Fig. 5. The control hardware for Minnesota robot

TABLE Experimentally identified inertial parameters for the university of Minnesota direct drive robot

	Parameters	Identified value	Computed value
	I_{z1}	0.19719	
(kg m^2)	I_{z2}	0.02592	
	$m_2x_2^2 + I_{e2} + I_{y2}$	1.68135	
	$m_2x_2^2 + I_{e2} + I_{z2}$	1.78135	
	$I_{e1} + I_{e5}$	0.28922	
	$I_{e1} + I_{e6}$	0.27759	
	I_{e3}	0.20	
	I_{e4}	0.14543	

program uses the measurements of the command voltage and the joint position of the robot. The accuracy of the dynamic parameters was experimentally verified via the comparison of the theoretically computed trajectories and the experimental trajectories. The identified dynamic parameters for the University of Minesota Direct Drive Robot are shown in Table I.

EXPERIMENTAL RESULTS

The preliminary evaluation of the performance of robot concerns the dynamic tracking accuracy along a specified trajectory. A feedforward compensator, as shown in Figure 6, is used to cancel the robot nonlinear terms while a set of constant gains are used in the feedback loop to decrease the error and develop robustness in modelling errors[19,20].

The reference trajectory in the experiment is generated by a cubic polynomial as shown in Figure 7. The dynamic model does not include the gravity terms because the University of Minnesota Robot is statically balanced. The robot control program, written in C language, yields a 250 Hz sampling frequency. All the joints were commanded to simultaneously move 30 degrees in 0.3 seconds from a predetermined origin. The maximum velocity and acceleration for each joint are 150 degree/sec and 2000 degree/sec^2, respectively.

The trajectory and velocity errors for each joint are depicted in Figures 8 and 9. Figure 8 shows the trajectory and velocity errors when all the robot parameters are calculated from the engineering drawings in Appendix B. The maximum tracking errors are 2.3°, 1.3°, and 2.3° for joint 1, 2 and 3, respectively.

Figure 9 shows the trajectory and velocity errors with the dynamic parameters identified experimentally. The trajectory and velocity errors are significantly reduced. The peak trajectory errors are 0.7°, 1.2° and 0.44° for joint 1, 2 and 3, respectively.

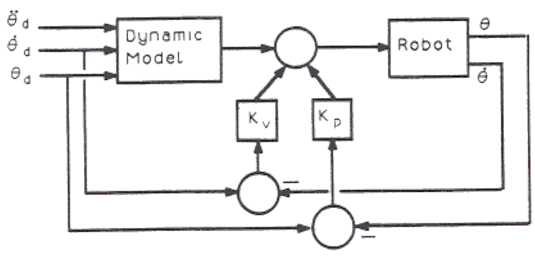

Fig. 6. The tracking controller [19, 20].

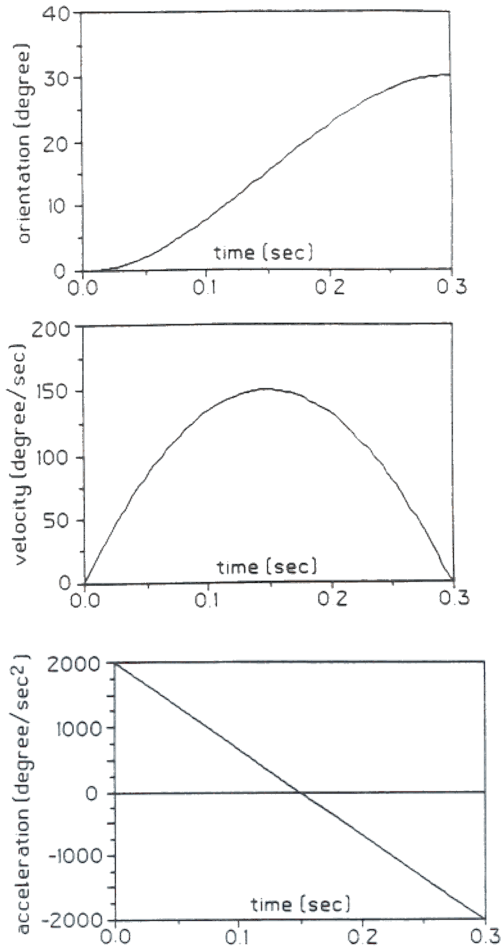

Fig. 7. Position, velocity, and acceleration profiles for a cubic polynomial trajectory.

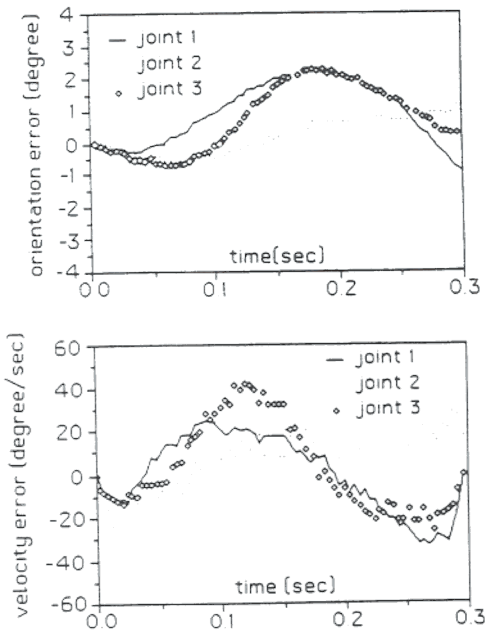

Fig. 8. Trajectory and velocity errors (all the parameters computed from the engineering drawings in Appendix B).

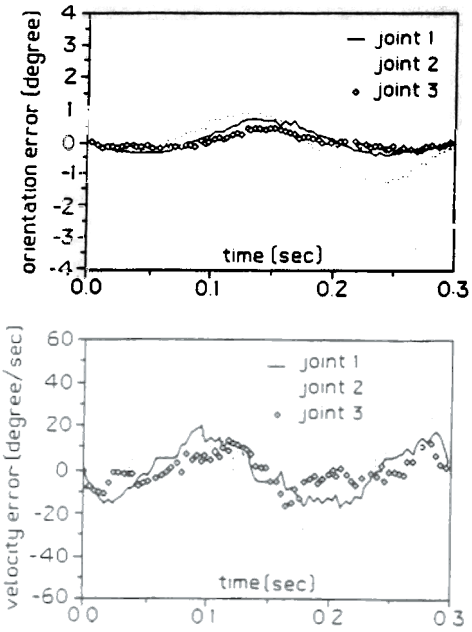

Fig. 9. Trajectory and velocity errors (all the parameters are experimentally identified).

APPENDIX A

A simple example in Figure A1 is given here to show that the transmission system does not necessarily result in lower speed for the output shaft. The dynamic equation describing the behavior of the system can be represented as:

$$\ddot{\theta}_2 = \frac{T}{(nI_1 + I_2/n)}$$

where (I_1, R_1, θ_1) and (I_2, R_2, θ_2) represent the moments of inertia, radius and orientation of each gear $(n = R_2/R_1)$. T is the motor torque. It is clear that the maximum acceleration will happen when n is chosen as:

$$n = \sqrt{I_2/I_1}$$

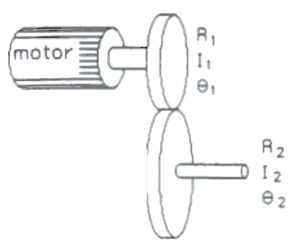

Fig. A1: Nondirect drive system.

APPENDIX B

Table B1 shows the values of robot parameters obtained from the engineering drawings. The uncertainty about the following parameters is about 10%.

TABLE B1. Robot Parameters

Link I	Length (cm)	$\bar{X}1$ (cm)	Mass (kg)	Inertia (kg cm 2) $Ix1$	$Iy1$	$Iz1$
1	—	—	—	—	—	1.752
2	60.33	−11.17*	13.886*	0.421*	3.7805*	3.7805*
3	53.34	15.70	3.206	0.0397	0.4796	0.4796
4	60.33	30.16	2.924	0.0207	1.3253	0.0
5	15.24	7.62	0.758	0.0016	0.0694	0.0694
g	22.23	—	—	—	—	—

* In the calculation of these values, we assume motor 3 is a part of link 2. For example 13.886 kg in the above table includes mass of link 2 (4.626 kg) and mass of motor 3 (9.26 kg). The "height" of the robot, from the base to the origin of the $X_1Y_1Z_1$, is 62.992 cm (24.8 inch).

CONCLUSION

This paper presents some results of the on-going research project on statically-balanced direct drive arm at the University of Minnesota. The following features characterize this robot:

1. The statically-balanced mechanism without counter weights allows for selection of smaller actuators. Since in static or quasi-static operations, no load is on the actuators, therefore the overheating of the previous direct drive robots is alleviated.
2. The robot links are made of graphite-epoxy composite materials to give more structural stiffness and less mass. The high structural stiffness and low mass of the links allow for the wide bandwidth of the control system.
3. To improve tracking errors, the robot parameters were identified experimentally. The errors in the trajectory and velocity were reduced significantly.

References

1. H. Kazerooni and S. Kim, "Statically Balanced Direct Drive Robot for Compliance Control Analysis", presented at *ASME Winter Annual Meeting, Modeling and Control of Robotic Manipulators and Manufacturing Processes* 193–201, Boston (1987).
2. N. Hogan, "Impedance Control, An Approach Manipulation", *ASME J. Dynamic Systems, Measurement, and Control* **107,** No. 1, 1–24 (March, 1985).
3. H. Kazerooni, T. B. Sheridan and P. K. Houpt, Fundamentals of Robust Compliant Motion for Robot Manipulators", *IEEE J. Robotics and Automation* **2,** No. 2, 83–92 (June, 1986).
4. H. Kazerooni, P. K. Houpt and T., B. Sheridan, "Design Method for Robust Compliant Motion for Robot Manipulators" *IEEE J. Robotics and Automation* **2,** No. 2, 93–105 (June, 1986).
5. H. Kazerooni and T. I. Tsay, "Stability Criteria for Robot Compliant Maneuvers", *In: Proceeding of the IEEE International Conference on Robotics and Automation, Philadelphia, PA,* **2,** 1166–1172 (April, 1988).
6. H. Kazerooni, "Direct-Drive Active Compliant End Effector (Active RCC)" *IEEE J. on Robotics and Automation,* **4,** No. 3, 324–333 (June, 1988).
7. H. Asada and T. Kanade, "Design of Direct Drive Mechanical arms" *ASME J. Vibration, Acoustics, Stress, and Reliability in Design* **105,** No. 3, pp. 312–316. (July 1983).
8. H. Asada and K. Youcef-Toumi, "Analysis and Design of a Direct Drive Arm with a Five-Bar-Link Parallel Drive Mechanism" *ASME J. Dynamic Systems, Measurement and Control,* **106,** No. 3, 225–230 (1984).
9. M.G. Forrest-Barlach and S.M. Babcock, "Inverse

Dynamics Position Control of a Compliant Manipulator", *IEEE* 1986 *International Conference on Robotics and Automation* **1,** pp. 196–205 (April, 1986).
10. E.I. Rivin, "Effective Rigidity of Robot Structures: Analysis and Enhancement" *Proceedings of* 85 *American Control Conference Boston, MA* **1,** 381–382 (1985).
11. J.J. Craig, *Introduction to Robotics*: *Mechanics and Control* (Addison-Wesley: Reading, Massachusetts, 1986).
12. K. Takase, T. Hasegawa and T. Suehiro, "Design and Control of a Direct Drive Manipulator" *Proceedings of the International Symposium on Design and Synthesis, Tokyo, Japan,* 333–338 (July 1984).
13. H. Kuwahara, Y. One, M. Nikaido and T. Matsumoto, "A Precision Direct Drive Robot Arm", In: *Proceedings of American Control Conference Boston, MA* **2,** 722–727 (1985).
14. S. Mahalingam and A.M. Sharan, "The Optimal Balancing of the Robotic Manipulators" *IEEE* 1986 *International Conference on Robotics and Automation, San Francisco, CA* **2,** 828–835 (April 1986).
15. H. Kazerooni and P.K. Houpt, "On the Loop Transfer Recovery", *Int. J. Control* **43,** No. 3, 981–996 (1986).
16. R.P. Paul, *Robot Manipulators*: *Mathematics, Programming, and Control* (MIT press, Cambridge, MA, 1981).
17. H. Asada, and J.-J.E. Slotine, *Robot Analysis and Control* (John Wiley and Sons New York, NY, 1986).
18. J.Y.S. Luh, M.W. Walker and R.P. Paul, "Resolved-Acceleration Control of Mechanical Manipulators" *IEEE Transactions on Automatic Control* **AC25,** No. 3, 468–474 (June, 1980).
19. C.H. An and C.G., J.D. Atkeson and J.M. Hollerbach, "Experimental Determination of the Effect of Feedforward Control on Trajectory Tracking Errors" *IEEE International Conference on Robotics and Automation, San Francisco, CA* **1,** 55–60 (April 1986).
20. H. Asada, T. Kanade, and I. Takeyama, "Control of a Direct Drive Arm" *J. Dynamic Systems, Measurements, and Control* **105,** 136–142 (September, 1983).